nanomaterials

MDPI

Article

Stepwise Splitting Growth and Pseudocapacitive Properties of Hierarchical Three-Dimensional Co_3O_4 Nanobooks

Huilong Chen [1], Shuang Lu [1], Feilong Gong [1], Huanzhen Liu [1] and Feng Li [2,*]

[1] State Laboratory of Surface and Interface Science and Technology, Zhengzhou University of Light Industry, Zhengzhou 450002, China; xunlingzhaohui@163.com (H.C.); ls102511@163.com (S.L.); longfei617381884@163.com (F.G.); huanzhenliuasd@sohu.com (H.L.)

[2] American Advanced Nanotechnology, Houston, TX 77459, USA

* Correspondence: lifeng696@yahoo.com or fengli@aananotech.com; Tel.: +86-371-6355-6510

Academic Editors: Bingqing Wei and Jian-Gan Wang

Received: 6 January 2017; Accepted: 4 April 2017; Published: 10 April 2017

Abstract: Three-dimensional hierarchical Co_3O_4 nanobooks have been synthesized successfully on a large scale by calcining orthorhombic $Co(CO_3)_{0.5}(OH)\cdot 0.11H_2O$ precursors with identical morphologies. Based on the influence of reaction time and urea concentration on the nanostructures of the precursors, a stepwise splitting growth mechanism can be proposed to understand the formation of the 3D nanobooks. The 3D Co_3O_4 nanobooks exhibit excellent pseudocapacitive performances with specific capacitances of 590, 539, 476, 453, and 421 F/g at current densities of 0.5, 1, 2, 4, and 8 A/g, respectively. The devices can retain ca. 97.4% of the original specific capacitances after undergoing charge–discharge cycle tests 1000 times continuously at 4 A/g.

Keywords: Co_3O_4; nanobooks; pseudocapacitors; stepwise splitting; hierarchical materials

1. Introduction

Cobalt cobaltite (Co_3O_4) is one of the most promising materials in designing advanced devices for storing energy, and its capacitive properties have been investigated extensively in the last decade [1–29]. It was found that 3D hierarchical Co_3O_4 nanoarchitectures exhibit excellent electrochemical performances due to their abilities of facilitating both fast electron transportation and ion diffusion [27–29]. Our group has concentrated on tailoring the microstructures of functional materials for improving their performances in storing energy [26–29]. Compared to single crystalline Co_3O_4 particles grown on and around multi-walled carbon nanotube (MWCNT) [26], for instance, porous and single crystalline Co_3O_4 beads show much better capacitive properties [29]. Three-dimensional nanoarchitectures constructed with 2D Co_3O_4 nanowalls exhibit outstanding performances in storing energy [27]. Based on a multistep splitting growth of 1D nanorods, Co_3O_4 twin-spheres with excellent pseudocapacitive properties can be produced on a large scale [28]. While we have expected that 2D nanosheets could also split in a manner similar to 1D nanorods behaving in the formation of twin-spheres with sea urchin like structures [28], to the best of our knowledge, there has to date been no report in the literature concerned with the synthesis and formation of 3D Co_3O_4 nanobooks.

Herein we endeavor to report on porous 3D Co_3O_4 nanobooks and their pseudocapacitive properties. One-dimensional $Co(CO_3)_{0.5}(OH)\cdot 0.11H_2O$ precursor nanorods can be initially generated in solvothermal reactions for their fast growth in the (100) direction. The 1D nanostructures then convert into 2D nanoplates with a prolonged reaction time. Finally, the 2D nanoplates split to form 3D hierarchical $Co(CO_3)_{0.5}(OH)\cdot 0.11H_2O$ nanoarchitectures with book-like structures. After annealing at

400 °C, 3D porous and hierarchical Co_3O_4 nanoarchitectures carrying the book-like morphologies of their precursors were produced successfully on a large scale. Based on the influence of reaction time and urea concentration on the nanostructures of the precursors, a stepwise splitting growth mechanism of 2D nanoplates can be proposed to understand the formation of the 3D hierarchical precursors. The pseudocapacitors fabricated with as-prepared materials exhibit excellent pseudocapacitive performances with specific capacitances of 590, 539, 476, 453, and 421 F/g at current densities of 0.5, 1, 2, 4, and 8 A/g, respectively. The devices can retain ca. 97.4% of the original specific capacitances after undergoing charge–discharge cycling 1000 times continuously at 4 A/g. The high specific capacitances, cycle stability, and the rate of the electrodes made with the Co_3O_4 nanobooks could be attributed to their special 3D nanostructures with nanosized pores.

2. Experimental

2.1. Chemicals and Characterization

All of the reagents were analytically pure and were purchased from Shanghai Chemical Industrial Co. Ltd. (Shanghai, China) and used without further purification. The morphologies of the as-prepared samples were investigated with field emission scanning electron microscopy (FESEM, JEOL JSM-7001F, 10 kV, Tokyo, Japan) and transmission electron microscopy (TEM, JEOL JEM-2100, 200 kV, Tokyo, Japan). The compositions of the materials were characterized with X-ray diffraction (XRD) analysis using a Bruker AXS D8 advance diffractometer with Cu Kα radiation (Bruker, Advanced D8, Karlsruhe, Germany). The N_2 adsorption and desorption isotherm was obtained using a Belsorp-Mini adsorption apparatus (Bel Japan Inc., Osaka, Japan). The pore size distribution was determined by using the BJH method applied to the desorption branch of adsorption–desorption isotherms.

2.2. Synthesis of Co_3O_4 Nanobooks

In a typical preparation, cobalt nitrate hexahydrate ($Co(NO_3)_2 \cdot 6H_2O$, 0.7271 g, 2.5 mmol) was first dissolved in 40 mL of a mix solvent consisting of ethylene glycol (EG, 20 mL) and deionized water (20 mL) to form a homogeneous solution under continuously stirring. Then, urea (NH_2CONH_2) (0.48 g, 8 mmol) was added into the solution. After stirring for another 30 min, the obtained solution was transferred into a Teflon-lined autoclave (50 mL) and kept at 160 °C for 20 h. After the autoclave was cooled naturally to room temperature, red powders were collected by centrifugation, washed with distilled water and ethanol 5 times each, and dried in vacuum at 60 °C for 12 h. Finally, the samples were calcined in a muffle furnace at 400 °C for 2 h in air, and then cooled to room temperature. The black powders of final products were collected for characterizations and applications.

2.3. Electrochemical Measurements

For the electrochemical measurements, active materials (Co_3O_4, 80 wt %), conductive material (acetylene carbon black, ATB, 10 wt %) and binder (polytetrafluoroethylene, PTFE, 10 wt %) were first mixed together and ground for ca. 10 min to obtain a mixture, which was then coated onto the surfaces of nickel meshes (ca. 1 × 1 cm) and dried at 100 °C for 12 h subsequently. The meshes with electrode materials (1.5 mg/cm) were finally pressed under 10 MPa to obtain working electrodes. The electrolyte used in the system was KOH aqueous solution (6 mol/L). All electrochemical measurements were carried out in a three-electrode experimental setup. Platinum foil and saturated calomel electrode (SCE) were used as counter electrode and reference electrode, respectively. Cyclic voltammogram (CV) was measured with an electrochemical workstation (CHI 660D, CH Instruments Inc., Shanghai, China). Galvanostatic charge–discharge cycle tests were performed on a LAND Cell test system CT2001A (Wuhan, China). The specific capacitances of the supercapacitors can be evaluated from the charge–discharge tests together with the following equation (Equation (1)) [1]:

$$C_m = I\Delta t / m\Delta V \quad (1)$$

where C_m is the specific capacitance of the capacitor (F/g), I is the current of the charge–discharge (A), and Δt is the discharging time period in seconds for the potential change ΔV. The m is the loaded mass of active materials. All of the electrochemical measurements were carried out at room temperature.

3. Results and Discussion

The precursors and final products were first characterized with XRD as shown in Figure 1. All of the identified peaks in Figure 1a can be indexed to orthorhombic cobalt carbonate hydroxide hydrate-$Co(CO_3)_{0.5}(OH)\cdot 0.11H_2O$ (JCPDS Card No. 48-0083, a = 0.886 nm, b = 1.012 nm and c = 0.444 nm). After annealing at 400 °C for 2 h, the precursors discomposed completely and convert from orthorhombic $Co(CO_3)_{0.5}(OH)\cdot 0.11H_2O$ into cubic Co_3O_4, as shown in Figure 1b. The XRD profile (Figure 1b) of the final materials confirms that the heat-treated samples only contain cubic Co_3O_4phase (JCPDS Card No. 42-1467, a = 0.8037). The high intensities of the peaks indicate that the as-prepared materials are well crystallized. No peaks are attributed to impurity in the pattern (5% deviation), which confirms the formation of single-phase $Co(CO_3)_{0.5}(OH)\cdot 0.11H_2O$ and Co_3O_4.

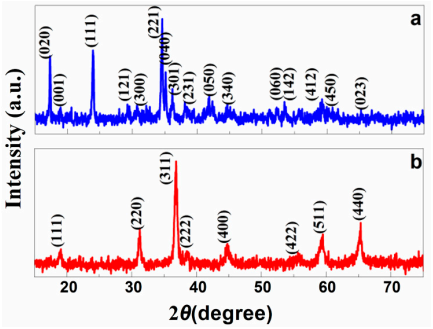

Figure 1. XRD profiles of (**a**) $Co(OH)_x(CO_3)_{0.5}\cdot 0.11H_2O$ and (**b**) Co_3O_4.

Figure 2a–c shows the FESEM images of as-prepared orthorhombic $Co(CO_3)_{0.5}(OH)\cdot 0.11H_2O$ precursors. Uniform and well-dispersed 3D hierarchical nanostructures (Figure 2a) consisting of rectangular nanoplates of ca. 10 and 8 μm in length and width, respectively, have been produced successfully. Higher magnification SEM images (Figure 2b,c) of the materials further reveal that the particles are mainly composed of 2D nanoplates of 2–5 generations growing out from the central area of nanoplate substrates to form 3D nanoarchitectures with book-like structures. The nanoplates with thicknesses ranging from 50 to 100 nm have smooth surfaces. In contrast, while the final Co_3O_4 materials obtained maintain the 3D hierarchical book-like morphology of the precursors, many pores are generated throughout the materials (Figure 2e,f) after they are annealed at 400 °C for 2 h. The porous nanostructures can be attributed to the decomposition of $Co(CO_3)_{0.5}(OH)\cdot 0.11H_2O$ precursor and the release of H_2O and CO_2 from the system.

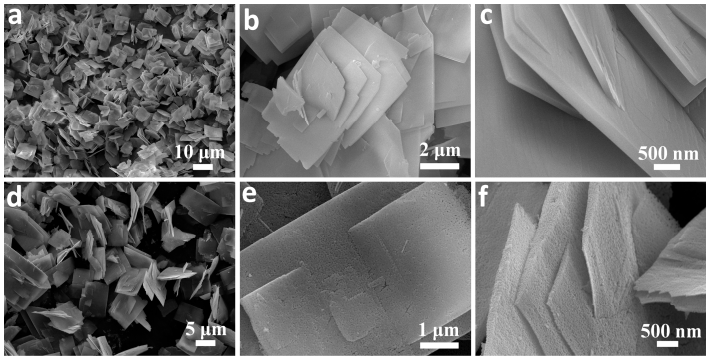

Figure 2. FESEM images of (**a**–**c**) $Co(CO_3)_{0.5}(OH)\cdot 0.11H_2O$ and (**d**–**f**) porous Co_3O_4 nanobooks.

More details concerned with the microstructures of the 3D precursor and porous Co_3O_4 nanobooks can be revealed by TEM and selective area electron diffraction (SAED). Figure 3a,b shows low magnification TEM images of several $Co(CO_3)_{0.5}(OH)\cdot 0.11H_2O$ nanobooks with smooth surfaces, which agrees well with the FESEM observations. The SAED pattern (insert in Figure 3b) composed of highly ordered dots, which can be attributed to the zone axis of (001) of orthorhombic $Co(CO_3)_{0.5}(OH)\cdot 0.11H_2O$ crystal phase, indicates that the nanoplates are single crystalline. The top and bottom planes of the nanoplates can therefore be indexed as the (001) plane of orthorhombic $Co(CO_3)_{0.5}(OH)\cdot 0.11H_2O$. Figure 3c shows a high-resolution TEM (HRTEM) image recorded near the edge of a precursor nanoplate. The measured d-spacings of 0.50 nm correspond to the (020) plane of orthorhombic $Co(CO_3)_{0.5}(OH)\cdot 0.11H_2O$. The results clearly verify that the orthorhombic $Co(CO_3)_{0.5}(OH)\cdot 0.11H_2O$ precursors grow in their (100) and (010) directions, respectively, to form rectangular nanoplates.

In contrast, the TEM image of the final Co_3O_4 nanobooks clearly shows porous structures across the particles. Many irregular pores from a few to tens of nanometers randomly distribute on the surface of the 3D Co_3O_4 nanobook as shown in Figure 3d,e. In addition, the TEM image as shown in Figure 3e reveals that the nanoplates consist of nanoparticles interconnected each other with a grain size of ca. 20 nm in diameter. The SAED pattern (inset in Figure 3e) of a Co_3O_4 nanoplate confirms the polycrystalline feature of the final products. The resolved fringes of 0.28 nm from the HRTEM image (Figure 3f) correspond to the (222) facet of cubic Co_3O_4.

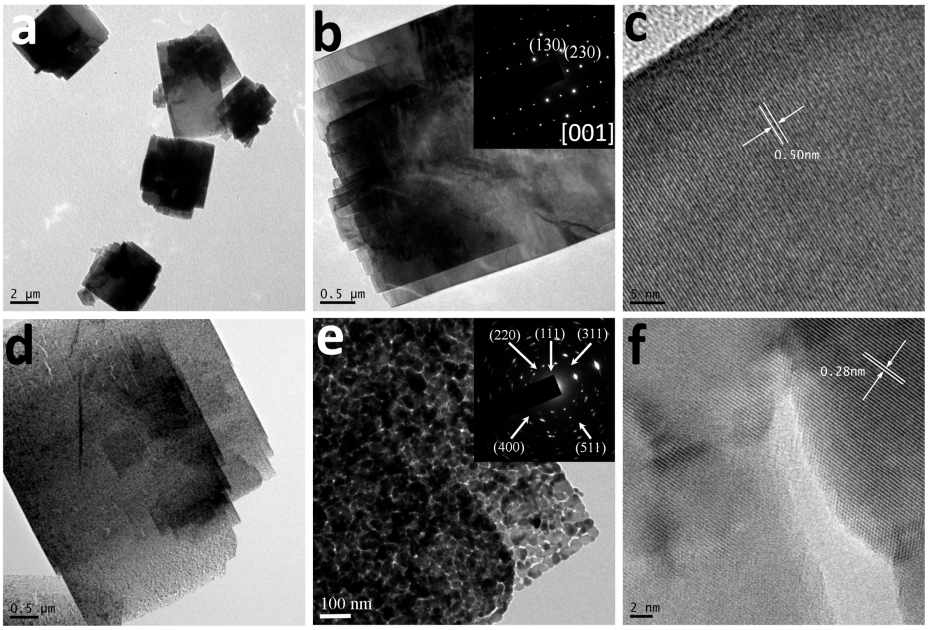

Figure 3. (**a**,**b**) TEM and (**c**) HRTEM images of single crystalline $Co(CO_3)_{0.5}(OH)\cdot 0.11H_2O$ nanobooks. (**d**,**e**) TEM and (**f**) HRTEM images of 3D hierarchical Co_3O_4 nanobooks. Insets in (**b**,**e**): the selective area electron diffraction (SAED) patterns of the precursor and final product.

The specific surface area and pore volume of Co_3O_4 nanobooks were measured by using N_2 adsorption and desorption experiments. Figure 4 shows the adsorption–desorption isotherm and the corresponding BJH pore size distribution plot (inset in Figure 4) of the materials. The existence of hysteresis loops between the isotherms indicates the adsorption–desorption characteristic of porous materials. The porous Co_3O_4 nanobooks with a total pore volume of 0.11 cm^3/g have a surface area of 19.45 m^2/g. Using the BJH method and desorption branch of nitrogen isotherm, we can calculate the size and shape of the pores, and the results indicate that the pores are not uniform in the Co_3O_4 nanobooks, and most of them are around 21.28 nm in diameter.

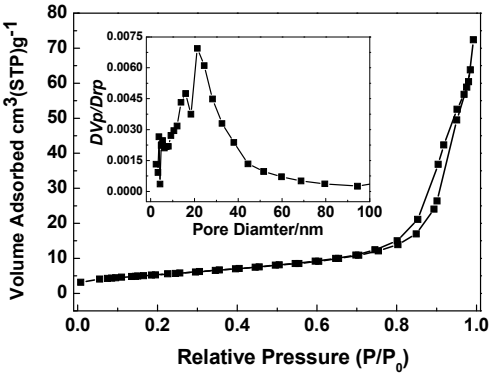

Figure 4. Typical nitrogen adsorption–desorption isotherm and pore-size distribution curve (inset) of Co_3O_4 nanobooks.

In order to understand the formation of the 3D hierarchical nanobooks, the reaction time effect on the morphology of the $Co(CO_3)_{0.5}(OH)\cdot 0.11H_2O$ precursor was carefully investigated by keeping the other reaction parameters identical. The structural evolution of the precursors is presented in Figure 5. One-dimensional nanorods of ca. 2 μm in length and 20 nm in diameter (Figure 5a) were first produced after reacting for 2 h. After prolonging the reaction time to 3 h, nanoplates appeared in the products (Figure 5b). More 2D nanoplates as shown in Figure 5c formed in the mixtures after reacting for 4 h. Many rectangular nanoplates were generated after 5 h of reaction, but nanorods still existed in the materials (Figure 5d). After performing the reaction for 6 h, the population of nanorods further reduced, in contrast to the generation of more nanoplates with a single layer (Figure 5e). Three-dimensional hierarchical nanobooks consisting of rectangular nanoplates with smooth surfaces (Figure 5f) were finally produced on a large scale, and the nanorods disappeared almost completely after conducting the reaction for up to 10 h. Based on the reaction time effect on the morphology of the precursors, it can be concluded safely that 3D hierarchical $Co(CO_3)_{0.5}(OH)\cdot 0.11H_2O$ nanobooks form at the expense of 1D nanorods.

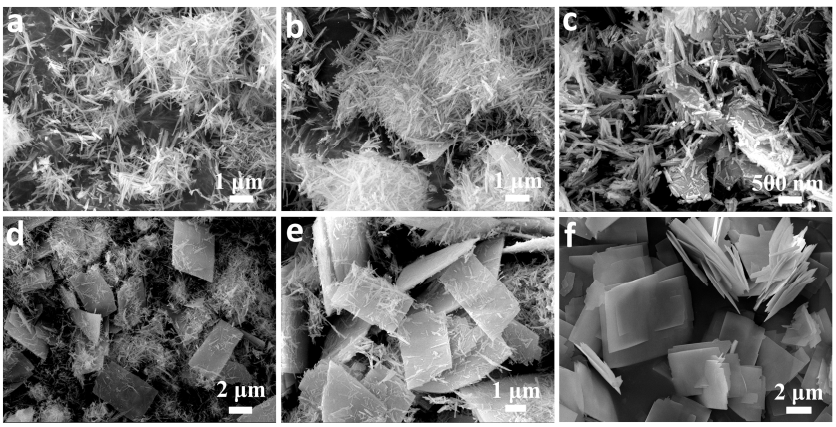

Figure 5. Morphology evolution of $Co(CO_3)_{0.5}(OH)\cdot 0.11H_2O$ precursors synthesized at 160 °C for (**a**) 2, (**b**) 3, (**c**) 4, (**d**) 5, (**e**) 6, and (**f**) 10 h, respectively.

Figure 6a,b shows the TEM and HRTEM image of a $Co(CO_3)_{0.5}(OH)\cdot 0.11H_2O$ nanorod of ca. 10 nm in diameter prepared by reacting for 2 h. The inset in Figure 6a depletes the SAED pattern of a whole nanorod as shown in Figure 6a. The measured d-spacings as shown in Figure 6a,c are 0.51 nm and 0.26 nm, respectively, which corresponds to the (020) and (320) lattice fringe of orthorhombic $Co(CO_3)_{0.5}(OH)\cdot 0.11H_2O$. These results indicate that $Co(CO_3)_{0.5}(OH)\cdot 0.11H_2O$ grow along its (100) axis to form single crystalline 1D nanorods. The orientations along the length, width, and thickness of

the rectangular precursor can therefore be indexed to be (100), (010), and (001), respectively. The fast growth of $Co(CO_3)_{0.5}(OH)\cdot 0.11H_2O$ in their (100) directions can generate 1D nanorods. The nanorods then grow in their (010) directions and further convert to 2D rectangular nanoplates in consuming the nanorods smaller in dimension due to Ostwald ripening. During the formation of rectangular nanoplates, the nucleate and growth can also take place at the central areas of the nanoplates for the higher energy in the regions. Many steps can therefore be generated in the central area of the nanoplates as shown in Figure 7a. The white arrow in the FESEM image (Figure 7b) of a nanobook further highlights the steps in its central area. Two nanoplates have fused perfectly together to form a 3D hierarchical nanobook, and the corresponding fringes and intersection angle agree well with the orthorhombic $Co(OH)_x(CO_3)_{0.5}\cdot 0.11H_2O$.

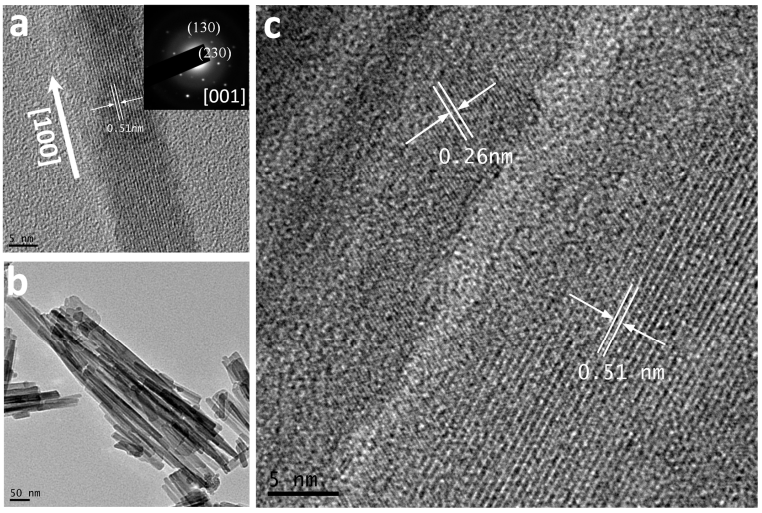

Figure 6. (**a**) HRTEM image of an individual $Co(CO_3)_{0.5}(OH)\cdot 0.11H_2O$ nanorod. (**b**) TEM image of $Co(CO_3)_{0.5}(OH)\cdot 0.11H_2O$ nanorods. (**c**) HRTEM image of two nanorods.

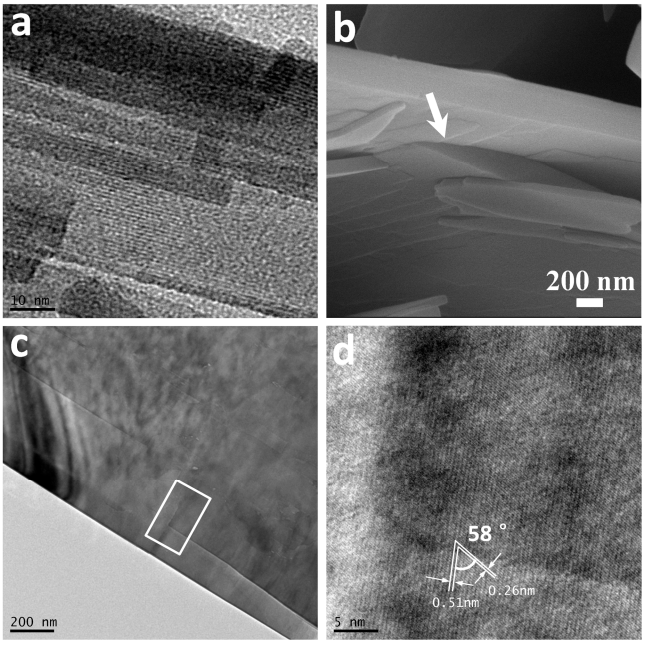

Figure 7. (**a**) TEM image of a $Co(CO_3)_{0.5}(OH)\cdot 0.11H_2O$ nanoplate with steps. (**b**–**d**) FESEM, TEM and HRTEM images at junction area of two nanoplates in a 3D hierarchical nanobook.

The effect of the urea on the nanostructures of the precursors was also investigated carefully by adding different amounts of the reactant into the reaction and keeping the other reaction parameters identical. Figure 8 shows the structure evolution of the precursors accompanying the increase of urea amount added to the reactions. Three-dimensional hierarchical nanospheres consisting of nanowires can be initially produced by adding a small amount of urea tothe reaction (Figure 8a). The structures of the products finally change into 3D nanobooks (Figure 8c) composed of 2D nanosheets after adding urea with a concentration of more than 6 mmol into the system. It has been pointed out that the carbonate and hydroxyl anions generated by the hydrolysis of urea can directly affect crystal growth [2]. The reactions involved in our system could be described as follows (Equations (2)–(5)):

$$NH_2CONH_2 + H_2O \rightarrow NH_3 + CO_2 \quad (2)$$

$$NH_3 + H_2O \rightarrow NH_4^+ + OH^- \quad (3)$$

$$CO_2 + H_2O \rightarrow CO_3^{2-} + 2H^+ \quad (4)$$

$$Co^{2+} + OH^- + CO_3^{2-} + 0.11H_2O \rightarrow Co(CO_3)_{0.5}OH{\cdot}0.11H_2O \quad (5)$$

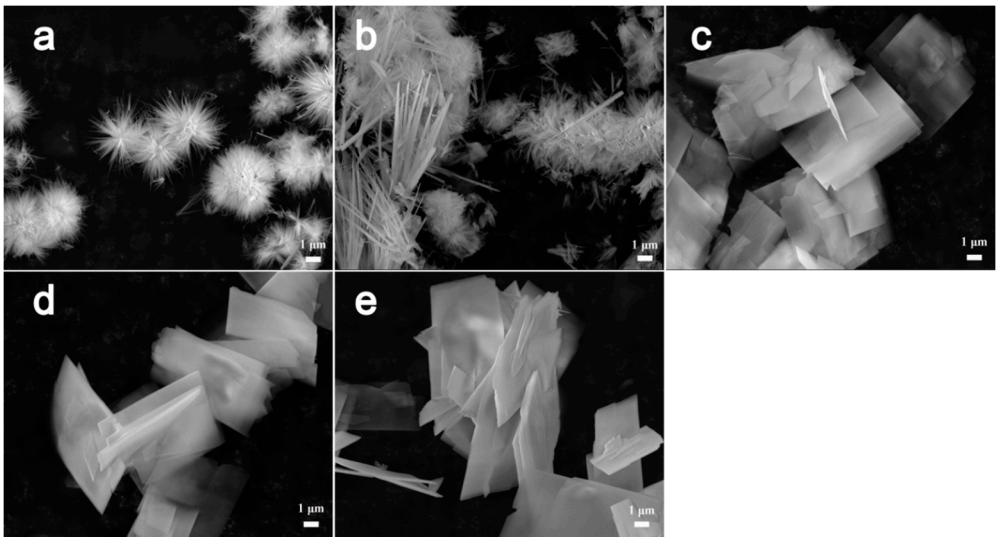

Figure 8. SEM images of precursors synthesized at 160 °C for 12 h by adding urea with (**a**) 1, (**b**) 3, (**c**) 6, (**d**) 10, and (**e**) 15 mmol intothe reactions, respectively.

The homogeneous formation of the precursors, which can be induced by the controlled generation of OH^- and CO_3^{2-} ions for the slow hydrolysis rate of urea, shows an apparent advantage in the structure control of final products in comparison with conventional preparations of materials based on precipitation. Urea has therefore also played an important role in controlling the nanostructures of the precursors.

Based on the experimental observation, a stepwise splitting growth (Figure 9) of 2D nanoplates can be proposed to understand the formation of the 3D nanobooks. One-dimensional nanorods can be initially produced in the reactions because of the highest energy of the (100) facets of orthorhombic $Co(CO_3)_{0.5}(OH){\cdot}0.11H_2O$ and thus their fast growth in the (100) direction (Figure 9a). However, the energy required to grow the crystals into longer 1D nanorods also increases as the nanorods lengthen. Consequently, the energy for growing precursor nanorods in (010) directions could finally catch up with the energy required for growing in the (100) direction. The nanorods therefore convert into 2D nanoplates with rectangular shape for the growths in both the (100) and (010) directions at the same time (Figure 9b) at the expense of nanorods with smaller sizes due to Ostwald ripening. The continued nucleation and growths of nanocrystals prefer to take place at the steps and defects on

their surfaces because of their higher energy in comparison to the smooth planes. The new generation of 2D nanoplates can therefore form at the central areas of the substrate nanoplates from the steps (Figure 9c). The stepwise growth of the nanoplates from the steps in the central areas of the nanoplate substrate eventually leads to the formation of 3D hierarchical materials with book-like structures (Figure 9d). It is still unclear, however, what has resulted in the 2D nanoplates orienting in directions that are different from those of the nanoplate substrates, while the perturbations could contribute to triggering the growth.

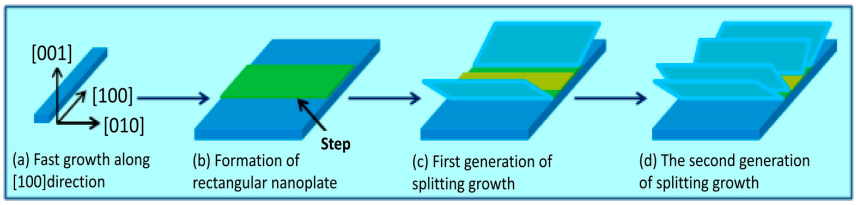

Figure 9. The multistep splitting growth of 3D hierarchical nanobook.

Co_3O_4 materials are promising candidates for designing supercapacitors for their relative low environmental foot print, low cost, and specific capacitance of 3560 F/g in theory. We made electrodes with as-prepared 3D Co_3O_4 nanobooks for testing their performances in storing energy. The electrochemical properties of the materials were first studied by cyclic voltammetry (CV) in a KOH electrolyte (6 mol/L) as shown in Figure 10a. The shapes of the CV curves are distinctly different from the CV curves of electrochemical double layer capacitors. Two pair of redox peaks can be observed during the anodic and cathodic sweeps, which correspond to the conversion between different oxidation states of cobalt according to Equations (6) and (7). The first redox couple A_1/C_1 corresponds to the conversion between CoOOH and Co_3O_4, and the second redox couple A_2/C_2 is attributed to the change between CoOOH and CoO_2. The plots of peak current density (I_p) versus square root of sweep rate (v) for cathodic peaks (Figure 10b) follow well a power-law relationship with the sweep rate ($I_p = av$). A b-value of 0.5 indicates that the current is controlled by semi-infinite linear diffusion, and a b-value of 1 shows that the current is surface-controlled. The electrode kinetics under the conditions investigated is a diffusion-controlled battery-type Faradaic process. The CV curves demonstrate the characteristic charge storage of the pseudocapacitive process originating from reversible redox reactions. It can also be observed that the potentials of the anodic and cathodic peaks shift toward more anodic and cathodic directions, respectively, as scan rates increase, which indicates the quasi-reversible feature of the redox couples.

$$Co_3O_4 + OH^- + H_2O \Leftrightarrow 3CoOOH + e \quad (6)$$

$$CoOOH + OH^- \Leftrightarrow CoO_2 + H_2O + e. \quad (7)$$

Figure 10c shows the galvanostatic charge–discharge curves of the supercapacitors made with porous Co_3O_4 nanobooks at different charge–discharge current densities with the potential window of −0.05–0.35 V. According to Equation (1), the discharge specific capacitance values (Figure 10d) of the porous Co_3O_4 nanobook electrodes calculated from the discharge curves are 590, 539, 476, 453, and 421 F/g at the current density of 0.5, 1, 2, 4, and 8 A/g, respectively. The decrease of the capacitances with the increase of the discharge current density is likely caused by the increase of the potential drop due to the resistance of the nanobooks and the relatively insufficient faradic redox reaction of active materials under higher discharge current densities. The specific capacitance value of the electrode retains ca. 71% and reaches 421 F/g at 8 A/g, compared to its value at 0.5 A/g. The excellent rate performances of porous Co_3O_4 nanobooks working at high current density are significant in practical applications of supercapacitors and could be attributed to the high efficiency of utilizing their active surface with nanosized pores and 3D hierarchical structures.

The cycle stability of supercapacitors is another crucial parameter for their practical applications. Figure 10e presents the cycling performances of the supercapacitors constructed with porous Co_3O_4 nanobooks under a current density of 4 A/g within the potential window of −0.05–0.35 V. A small decrease of specific capacitance can be observed after being cycled 300 times, which could be due to the consumption of electrode materials and binder for the redox taking place on the surface of the electrode. The capacitances of the devices remain almost constant after that, and they can retain approximately 97.4% of their maximum values after being cycled 1000 times. The results show the excellent stability of the electrodes assembled with 3D Co_3O_4 nanobooks. The galvanostatic curves (inset in Figure 10e) of the materials at the current density of 4 A/g show that the charge–discharge process of the electrode is highly reversible. Compared to the Co_3O_4 nanowires [7], hexagonal platelets [11], porous nanoplates [22], monolayer hollow spheres [12], nanorod assembled nanospheres [15], and porous particles [16] reported in the literature, as-prepared nanobooks show much higher specific capacitance at a high current density of 8 A/g. Our Co_3O_4 nanobooks also show comparable specific capacitance to hollow fluffy cages [1], porous nanostructures [14], twin-spheres [28], and hierarchical nanoarchitectures [27]. The materials also exhibit much higher specific capacitances in comparison with MoS_2 [30] and α-Fe_2O_3 [31], and they are also comparable to CoS_2 [32] and $NiCo_2S_4$ [33]. We could further improve the electrochemical performances of our nanobooks through constructing hybrids with carbon materials or transitional metal sulfides [34]. It was found that the microstructures, including their sizes and pores, affect their electrochemical performances dramatically, and we can also tailor the structures of the materials by adjusting the reaction parameters, thus improving their capabilities in storing energy.

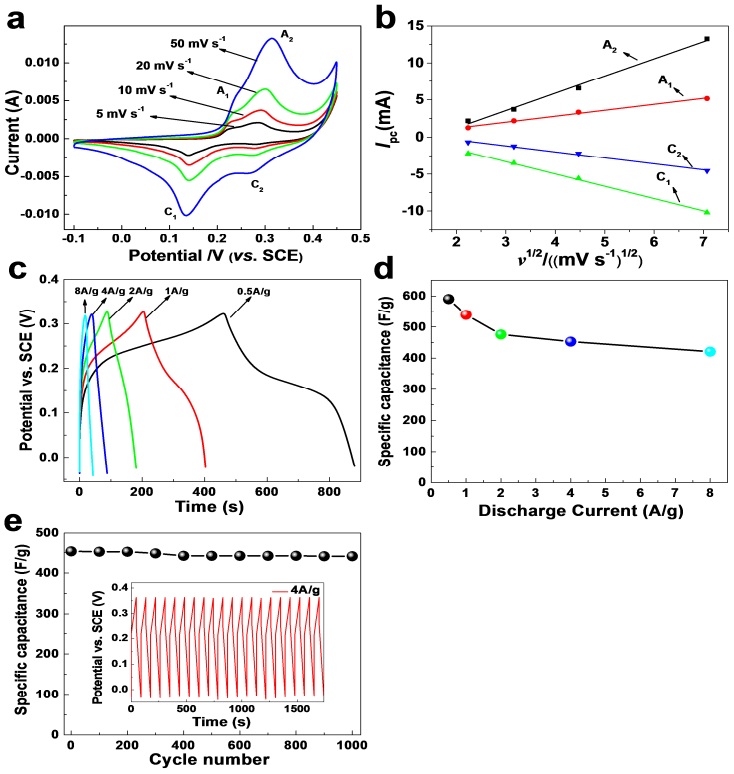

Figure 10. (**a**) CV of Co_3O_4 nanobooks in KOH electrolyte and (**b**) the relationship between the CV peak current (I_p) and the square root of the scan rate (v). (**c**) Charge-discharge curves of porous Co_3O_4 nanoplates in KOH electrolyte (6 mol/L). (**d**) Average specific capacitances of the supercapacitors at different discharge current densities. (**e**) Average specific capacitances versus cycle number of the devices at galvanostatic charge and discharge current density of 4 A/g. The inset shows galvanostatic charge–discharge curves of the devices constructed with porous Co_3O_4 nanoplates at current density of 4 A/g.

4. Conclusions

In summary, we have successfully demonstrated an approach for the scalable synthesis of porous 3D hierarchical Co_3O_4 nanobooks, based on a stepwise splitting growth of 2D nanoplates. The supercapacitors made with the materials show excellent electrochemical performances in rate and stability, which could be attributed to the porous 3D hierarchical structure of the nanobooks. By simply adjusting the reaction parameters, one can tailor the microstructures of the electrode materials and tune their electrochemical properties effectively. The stepwise splitting growth of 2D nanoplates could open a new pathway for constructing 3D hierarchical materials storing energy.

Acknowledgments: The authors are grateful to the financial support from the National Natural Science Foundation of China (NSFC. 21071130 and 21371157), the Outstanding Scholar Program of Henan Province (114200510012), and the Key Program of Henan Province for Science and Technology (132102210424).

Author Contributions: H. Chen worked on materials synthesis, characterization and their electrochemical properties. H. Chen also wrote the paper. S. Lu contributed to synthesize materiald and assemble supercapacitors; F. Gong helped to characterize the materials; H. Liu measured the electrochemical properties; F. Li designed the experiments, directed the researches, analyzed the data, proposed the formation mechanism, and wrote the paper.

Conflicts of Interest: All of the authors have agreed to publish the paper and there is no conflict of interests.

References

1. Zhou, X.; Shen, X.; Xia, Z.; Zhang, Z.; Li, J.; Ma, Y.; Qu, Y.; Cen, Q. Hollow fluffy Co_3O_4 cages as efficient electro-active materials for supercapacitors and oxygen evolution reaction. *ACS Appl. Mater. Interfaces* **2015**, *7*, 20322–20331. [CrossRef] [PubMed]
2. Wang, H.; Zhang, L.; Tan, X.; Holt, C.M.B.; Zahiri, B.; Olsen, B.C.; Mitlin, D. Supercapacitive properties of hydrothermally synthesized Co_3O_4 nanostructures. *J. Phys. Chem. C* **2011**, *115*, 17599–17605. [CrossRef]
3. Wang, D.; Wang, Q.; Wang, T. Morphology-controllable synthesis of cobalt oxalates and their conversion to mesoporous Co_3O_4 nanostructures for application in supercapacitors. *Inorg. Chem.* **2011**, *50*, 6482–6492. [CrossRef] [PubMed]
4. Xuan, L.; Chen, L.; Yang, Q.; Chen, W.; Hou, X.; Jiang, Y.; Zhang, Q.; Yuan, Y. Engineering 2D multi-layer graphene-like Co_3O_4 thin sheets with vertically aligned nanosheets as basic building units for advanced pseudocapacitor materials. *J. Mater. Chem. A* **2015**, *3*, 17525–17533. [CrossRef]
5. Yuan, C.; Yang, L.; Hou, L.; Shen, L.; Zhang, X.; Lou, X.W. Growth of ultrathin mesoporous Co_3O_4 nanosheetarrays on Ni foam for high-performance electrochemical capacitors. *Energy Environ. Sci.* **2012**, *5*, 7883–7887. [CrossRef]
6. Hu, H.; Guan, B.; Xia, B.; Lou, X.W. Designed formation of Co_3O_4/$NiCo_2O_4$ double-shelled nanocages with enhanced pseudocapacitive and electrocatalytic properties. *J. Am. Chem. Soc.* **2015**, *137*, 5590–5595. [CrossRef] [PubMed]
7. Wang, B.; Zhu, T.; Wu, H.B.; Xu, R.; Chen, J.S.; Lou, X.W. Porous Co_3O_4 nanowires derived from long $Co(CO_3)_{0.5}(OH)\cdot 0.11H_2O$ nanowires with improved supercapacitive properties. *Nanoscale* **2012**, *4*, 2145–2149. [CrossRef] [PubMed]
8. Zhu, T.; Chen, J.S.; Lou, X.W. Shape-controlled synthesis of porous Co_3O_4 nanostructures for application in supercapacitors. *J. Mater. Chem.* **2010**, *20*, 7015–7020. [CrossRef]
9. Zhang, F.; Yuan, C.; Zhu, J.; Wang, J.; Zhang, X.; Lou, X.W. Flexible films derived from electrospun carbon nanofibers incorporated with Co_3O_4 hollow nanoparticles as self-supported electrodes for electrochemical capacitors. *Adv. Funct. Mater.* **2013**, *23*, 3909–3915. [CrossRef]
10. Ning, F.; Shao, M.; Zhang, C.; Xu, S.; Wei, M.; Duan, X. Co_3O_4@layered double hydroxide core/shell hierarchical nanowire arrays for enhanced supercapacitance performance. *Nano Energy* **2014**, *7*, 134–142. [CrossRef]
11. Deori, K.; Ujjain, S.K.; Sharma, R.K.; Deka, S. Morphology controlled synthesis of nanoporous Co_3O_4 nanostructures and their charge storage characteristics in supercapacitors. *ACS Appl. Mater. Interfaces* **2013**, *5*, 10665–10672. [CrossRef] [PubMed]
12. Xia, X.-H.; Tu, J.-P.; Wang, X.-L.; Gu, C.-D.; Zhao, X.-B. Mesoporous Co_3O_4 monolayer hollow-sphere array as electrochemical pseudocapacitor material. *Chem. Commun.* **2011**, *47*, 5786–5788. [CrossRef] [PubMed]

13. Rakhi, R.B.; Chen, W.; Cha, D.; Alshareef, H.N. Substrate dependent self-organization of mesoporous cobalt Oxide nanowires with remarkable pseudocapacitance. *Nano Lett.* **2012**, *12*, 2559–2567. [CrossRef] [PubMed]
14. Zhang, Y.-Z.; Wang, Y.; Xie, Y.-L.; Cheng, T.; Lai, W.-Y.; Pang, H.; Huang, W. Porous hollow Co_3O_4 with rhombic dodecahedral structures for high-performance supercapacitors. *Nanoscale* **2014**, *6*, 14354–14359. [CrossRef] [PubMed]
15. Wang, Y.; Pan, A.; Zhu, Q.; Nie, Z.; Zhang, Y.; Tang, Y.; Liang, S.; Cao, G. Facile synthesis of nanorod-assembled multi-shelled Co_3O_4 hollow microspheres for high-performance supercapacitors. *J. Power Sources* **2014**, *272*, 107–112. [CrossRef]
16. Meng, F.; Fang, Z.; Li, Z.; Xu, W.; Wang, M.; Liu, Y.; Zhang, J.; Wang, W.; Zhao, D.; Guo, X. Porous Co_3O_4 materials prepared by solid-state thermolysis of a novel Co-MOF crystal and their superior energy storage performances for supercapacitors. *J. Mater. Chem. A* **2013**, *1*, 7235–7241. [CrossRef]
17. Kung, C.-W.; Chen, H.-W.; Lin, C.-Y.; Vittal, R.; Ho, K.-C. Synthesis of Co_3O_4 nanosheets via electrodeposition followed by ozone treatment and their application to high-performance supercapacitors. *J. Power Sources* **2012**, *214*, 91–99. [CrossRef]
18. Jena, A.; Munichandraiah, N.; Shivashankar, S.A. Morphology controlled growth of meso-porous Co_3O_4 nanostructures and study of their electrochemical capacitive behavior. *J. Electrochem. Soc.* **2012**, *159*, A1682–A1689. [CrossRef]
19. Zhang, G.; Wang, T.; Yu, X.; Zhang, H.; Guan, H.; Lu, B. Nanoforest of hierarchical Co_3O_4@$NiCo_2O_4$ nanowire arrays for high-performance supercapacitors. *Nano Energy* **2013**, *2*, 586–594. [CrossRef]
20. Liu, J.; Jiang, J.; Cheng, C.; Li, H.; Zhang, J.; Gong, H.; Fan, H.J. Co_3O_4 nanowire@MnO_2 ultrathin nanosheet core/shell arrays: A new class of high-performance pseudocapacitive materials. *Adv. Mater.* **2011**, *23*, 2076–2081. [CrossRef] [PubMed]
21. Xiong, S.; Yuan, C.; Zhang, M.; Xi, B.; Qian, Y. Controllable synthesis of mesoporous Co_3O_4 nanostructures with tunable morphology for application in supercapacitors. *Chem. Eur. J.* **2009**, *15*, 5320–5326. [CrossRef] [PubMed]
22. Razmjoo, P.; Sabour, B.; Dalvand, S.; Aghazadeh, M.; Ganjali, M.R. Porous Co_3O_4 nanoplates: Electrochemical synthesis, characterization and investigation of supercapacitive performance. *J. Electrochem. Soc.* **2014**, *161*, D293–D300. [CrossRef]
23. Fan, Y.; Shao, G.; Ma, Z.; Wang, G.; Shao, H.; Yan, S. Ultrathin nanoflakes assembled 3D hierarchical mesoporous Co_3O_4 nanoparticles for high-rate pseudocapacitors. *Part. Part. Syst. Charact.* **2014**, *31*, 1079–1083. [CrossRef]
24. Yang, W.; Gao, Z.; Ma, J.; Wang, J.; Wang, B.; Liu, L. Effects of solvent on the morphology of nanostructured Co_3O_4 and its application for high-performance supercapacitors. *Electrochim. Acta* **2013**, *112*, 378–385. [CrossRef]
25. Yuan, C.; Yang, L.; Hou, L.; Shen, L.; Zhang, F.; Li, D.; Zhang, X. Large-scale Co_3O_4 nanoparticles growing on nickel sheets via a one-step strategy and their ultra-highly reversible redox reaction toward supercapacitors. *J. Mater. Chem.* **2011**, *21*, 18183–18185. [CrossRef]
26. Xiao, Y.; Liu, S.; Fang, S.; Jia, D.; Su, H.; Zhou, W.; Wiley, J.B.; Li, F. Plum-like and octahedral Co_3O_4 single crystals on and around carbon nanotubes: Large scale synthesis and formation mechanism. *RSC Adv.* **2012**, *2*, 3496–3501. [CrossRef]
27. Xiao, Y.; Zhang, A.; Liu, S.; Zhao, J.; Fang, S.; Jia, D.; Li, F. Free-standing and porous hierarchical nanoarchitectures constructed with cobalt cobaltite nanowalls for supercapacitors with high specific capacitances. *J. Power Sources* **2012**, *219*, 140–146. [CrossRef]
28. Xiao, Y.; Liu, S.; Li, F.; Zhang, A.; Zhao, J.; Fang, S.; Jia, D. 3D hierarchical Co_3O_4 twin-spheres with an urchin-like structure: Large-Scale synthesis, multistep-splitting growth and electrochemical pseudocapacitors. *Adv. Funct. Mater.* **2012**, *22*, 4052–4059. [CrossRef]
29. Gong, Y.; Gong, F.; Wang, C.; Zheng, H.; Li, F. Porous and single crystalline Co_3O_4 nanospheres for pseudocapacitors with enhanced performance. *RSC Adv.* **2015**, *5*, 27266–27272. [CrossRef]
30. Wang, X.; Ding, J.; Yao, S.; Wu, X.; Feng, Q.; Wang, Z.; Geng, B. High supercapacitor and adsorption behaviors of flower-like MoS_2 nanostructures. *J. Mater. Chem. A* **2014**, *2*, 15958–15963. [CrossRef]
31. Xin, Z.; Yan, X.; Sun, Y.; Yu, Y.; Zhang, G.; Shen, Y.; Liang, Q.; Liao, Q.; Yue, Z. Temperature-dependent electrochemical capacitive performance of the α-Fe_2O_3 hollow nanoshuttles as supercapacitor electrodes. *J. Colloid Interface Sci.* **2016**, *466*, 291–296.

32. Pujari, R.B.; Lokhande, A.C.; Kim, J.H.; Lokhande, C.D. Bath temperature controlled phase stability of hierarchical nanoflakes CoS_2 thin films for supercapacitor application. *RSC Adv.* **2016**, *6*, 40593–40601. [CrossRef]
33. Guan, B.Y.; Yu, L.; Wang, X.; Song, S.; Lou, X.W. Formation of onion-like $NiCo_2S_4$ particles via sequential ion-exchange for hybrid supercapacitors. *Adv. Mater.* **2017**, *29*, 1605051. [CrossRef] [PubMed]
34. Zhou, H.; Zhang, L.; Zhang, D.; Chen, S.; Coxon, P.R.; He, X.; Coxon, P.R.; He, X.; Coto, M.; Kim, H.K. A universal synthetic route to carbon nanotube/transition metal oxide nano-composites for lithium ion batteries and electrochemical capacitors. *Sci. Rep.* **2016**, *6*, 37752. [CrossRef] [PubMed]